JMEPEG (2011) 20:1575–1582
DOI: 10.1007/s11665-010-9829-4

1059-9495/$19.00

Effect of Mg on the Microstructure and Mechanical Properties of Al0.3Sc0.15Zr-TiB_2 Composite

A.K. Lohar, B.N. Mondal, and S.C. Panigrahi

(Submitted June 23, 2010; in revised form October 27, 2010)

Al-0.3Sc-0.15Zr-TiB_2 composites with varying additions of Mg were cast through a novel processing technique using oil Quenched Investment Casting (QIC). Addition of Mg resulted in grain refinement of the composite. Al_3(Sc, Zr) primary particles and TiB_2 are responsible for grain refinement in these composites. Presence of fine nanosized uniformly distributed precipitates of Al_3(Sc, Zr) at the peak age condition together with TiB_2 particles increase the strength and ductility of the composites. The presence of Sc and Zr reduces the size of TiB_2 particles down to 10 nm. The optimum magnesium content in the composites studied lies between 3.5 and 6%.

Keywords Al-Mg alloy, Al-Sc and Al-Zr, grain refinement, TiB_2 particles

1. Introduction

Increased demand of materials with higher mechanical properties in terms of higher strength to weight and cost ratio have led to the development of several aluminum alloys and composites based on these alloys. The reinforcement particles produced by in situ synthesis have several advantages over ex situ particulate reinforced metal matrix composites. The poor wettability, inhomogeneous distribution, and reaction products at the interface between matrix and particles are the main drawbacks of ex situ composites. This has led to the development of several in situ particles reinforced aluminum matrix composites. Aluminum-based composites reinforced with TiB_2 particles exhibits excellent mechanical and tribological properties due to high stiffness and hardness of submicron size particles (Ref 1-3). Among the several techniques for introducing TiB_2 particles in the matrix of aluminum, use of alumino-thermic reduction of complex fluorides like K_2TiF_6 and KBF_4 is well established (Ref 4-6). The particles produced by the reaction are rapidly dispersed in the liquid aluminum alloy and refine the grain structure during solidification. A uniform dispersion of reinforcement particle in the matrix in a composite is one of the factors for getting improved mechanical properties. Magnesium addition to the aluminum matrix composite reduces the interfacial energy and help in dispersing the particles uniformly in the matrix and accelerating the nucleation rate of the TiB_2 particles during reaction (Ref 7, 8). The structure refinement with TiB_2 particles depends on the reaction time (Ref 9), the presence of free Ti in the melt (Ref 10), solidification velocity (Ref 11), and mechanical agitation (Ref 12, 13). Particles settling and agglomeration at the long holding time influence the grain refining performance (Ref 14). In the presence of Zr poisoning of the grain refining effect has been observed which is attributed to the reduction of the effectiveness of TiB_2. The mechanism of poisoning TiB_2 by Zr is not very clear but partial substitution of Zr for Ti in Al_3Ti layer on the TiB_2 particle is the most accepted reason for the destruction of the grain refining potency of TiB_2 (Ref 15).

Matrix of the composite material plays an important role for the contribution to the strength properties. There have been extensive investigations on the Sc-containing aluminum alloys with regard to the grain refining performance (Ref 16) and aging behavior (Ref 17-20). The grain structure modification is much superior with the addition of Sc when compared to the commercial Al-5Ti-1B alloy (Ref 21). Zr is added to these alloys to reduce the Sc content to reduce the cost. Zr addition significantly influences the aging response and results in the improvement of mechanical properties through precipitation of nanosized Al_3Sc/Al_3(Sc, Zr) phase after aging. Mg addition to the ternary Al-Sc-Zr alloy gives rise to a significant solid solution strengthening (Ref 22).

Extensive research on the Sc-containing aluminum alloys and TiB_2 reinforced aluminum alloy composites is reported but very little information is available on the performance of the Sc- and Zr-containing Al alloy reinforced with TiB_2. The focus of the present investigation is to study Al-Sc-Zr/TiB_2 composite with different Mg contents. The other cast alloys containing Cu and Si are avoided as in these alloys reduce the available Sc for the nucleation of the nanosized coherent precipitates of Al_3Sc by the formation of W-phase (AlCuSc) and V phase ($AlSc_2Si_2$) (Ref 22). Sc-containing aluminum alloys, besides composition cooling rate is an important parameter to control effectively the Sc available for precipitation strengthening. Increase in the cooling rate increases the number of particles and increase in the number of potent nucleation sites.

There are several advantages for producing component in the well-known Investment casting process. In the Investment casting process, more clustering of the particles at the grain boundary because of particle pushing and a decrease in the number of particles is expected due to the prevailing slow

A.K. Lohar and **B.N. Mondal**, CAMP, CMERI (CSIR), Durgapur 713209, India; and **S.C. Panigrahi**, Department of Metallurgy and Materials Engineering, IIT, Kharagpur, India. Contact e-mail: adityalohar@yahoo.co.in.

cooling rates. A higher cooling rate was achieved in this study by quenching the investment shell in a preheated oil bath immediately after pouring to avoid these difficulties. The objective of this study is to study the influence of Mg on the precipitation morphology and mechanical properties of TiB_2 particle reinforced cast Al-0.3Sc-0.15Zr composite.

2. Experimental Procedure

In this study, Al-0.3Sc-0.15Zr alloy was prepared by diluting Al-2Sc and Al-10Zr master alloys with commercial purity aluminum (99.7%). TiB_2 was allowed to form by in situ reaction of K_2TiF_6 and KBF_4 salt mixture at 800 °C for 60 min. The composite melt was stirred for 2 min with a graphite blade stirrer at an interval of 10 min. The masses for the salts were calculated in the atomic ratio in accordance with Ti/2B for a selected dispersion of 5 wt.% TiB_2. A calculated amount of magnesium (99.9%) ribbon considering loss of Mg (17%) experimentally observed during melting was added 10 min before pouring. The molten composite was poured into the investment shell mold, which was quenched immediately after pouring into an oil bath. This process is subsequently referred as QIC (Ref 23). Shrinkage at the casting wall was observed at the combination of low temperature of oil and molten metal. To avoid casting defects the pouring temperature was maintained about 700 °C and oil temperature of 100 °C. The cooling rate achieved in this process was 5.93 °C/s. Quenching was done to increase the solidification rate. Cylindrical samples of 220 mm length and 25 mm diameter were produced by this process.

Microstructure of the samples collected from the casting was examined with optical, scanning electron microscope (SEM), and transmission electron microscope (TEM). Aging of the as-cast samples were carried out at 300 and 400 °C for different lengths of time. After aging, samples were quenched in water at room temperature to prevent solid-state reaction. The samples aged at 300 °C for 5 h were tested for tensile strength. Although the peak age hardness was reached in between 90 and 150 min, aging was carried for a longer period at the temperature of 300 °C to allow the completion of solid-state reaction. All the five sets of tensile tests of the composite samples showed consistent result. Figure 1 shows the dimensions of the tensile specimen. The tensile test was done in TINIUS OLSEN make HK50-S UTM. The tensile tests were performed at 1 mm/min crosshead speed.

The overall Mg, Fe, Zr, and Si contents were determined with the aid of the optical emission spectroscopy (OES) in SPECTRU MAT 750 from LECO. Sc content shown is nominal. The values of Ti could not be quantified experimentally with sufficient precision because of lacking standards. Mg content was varied and the chemical composition of the composites made is shown in Table 1. Local chemical analysis

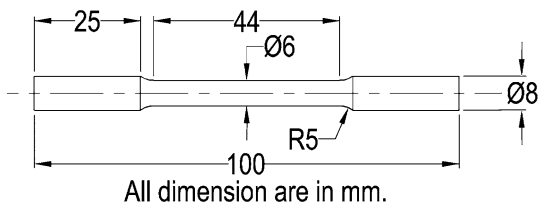

Fig. 1 Schematic diagram of the tensile specimen

was performed using scanning electron microscopy with energy dispersive x-ray spectroscopy (SEM/EDX). Microstructure of the samples was investigated using both optical (OM) and scanning electron microscopy (SEM). Grain size was measured by linear intercept method by QWin image processing and analysis toolkit from LEICA. A special effort was made to identify Al_3Sc precipitates. For optical and electron microscopy, the samples were mechanically polished and final polishing was done using Sadbhav metallurgical services make INSIPOL 2000 portable electrolytic polisher. Etching treatment with Keller's reagent was not done as nitric acid was found to attack Al_3Sc phase chemically and to cause problems during micro-chemical analysis via EDX. Attempt was made to identify Sc precipitates in the as-cast microstructure of the SEM samples. The microchemical analysis was carried out in the SEM with EDX on the unetched samples. Transmission electron microscopy (TEM) was performed using a JEM-2100 HRTEM, Japan with Energy Dispersive x-ray (EDX) Analyzer (Make-Oxford Instruments, UK). To analyze the nanosized precipitates in the as-cast sample, TEM samples were prepared using the precision ion polishing system from Gatan. Ion beam polishing was carried out so as to avoid electrochemical polishing, which uses nitric acid and methanol mixture that chemically attacked Al_3Sc precipitates. Hardness measurements were done using a Vickers hardness-testing machine with applied load of 10 kg for 15 s. X-ray diffraction study was carried out in XPERT-Pro diffractometer from PANalytical B. V., Almelo, Netherland. A Cu-target x-ray source was used in this study.

3. Results

3.1 As-Cast Microstructure

Microstructures of the samples cast in QIC are shown in Fig. 2. Figure 2(a) shows the optical microstructure of the sample without magnesium. It reveals the typical banded structure with an average grain size of 135 μm. With addition of 1.5% Mg the banded structure disappeared and the grain size is finer as seen in Fig. 2(b). With further increase in Mg grain size increased. The average grain size, as measured by linear intercept method, is 27, 40, 45 μm, respectively, for the composites containing 1.5, 3.5, and 6 wt.% Mg. There was marginal increase in grain size when the magnesium was increased from 3.5 to 6% as seen from Fig. 2(d). TiB_2 particles are normally seen at the grain boundaries. The decrease in grain boundary area means there is an increase in particle density with volume fraction of the reinforcement remaining same. The change in contrast of the optical micrograph indicates the increase in particle density, which is noticeable with increase in

Table 1 Chemical composition (in wt.%) of the alloys

Alloy	Mg	Sc (nominal)	Fe	Si	Ti (a)	Zr	Al
0.0 Mg	…	0.3	0.20	0.26	…	0.14	Bal.
1.5 Mg	1.63	0.3	0.25	0.24	…	0.13	Bal.
3.5 Mg	3.40	0.3	0.21	0.26	…	0.16	Bal.
6.0 Mg	6.08	0.3	0.22	0.26	…	0.15	Bal.

(a) Lack in standard

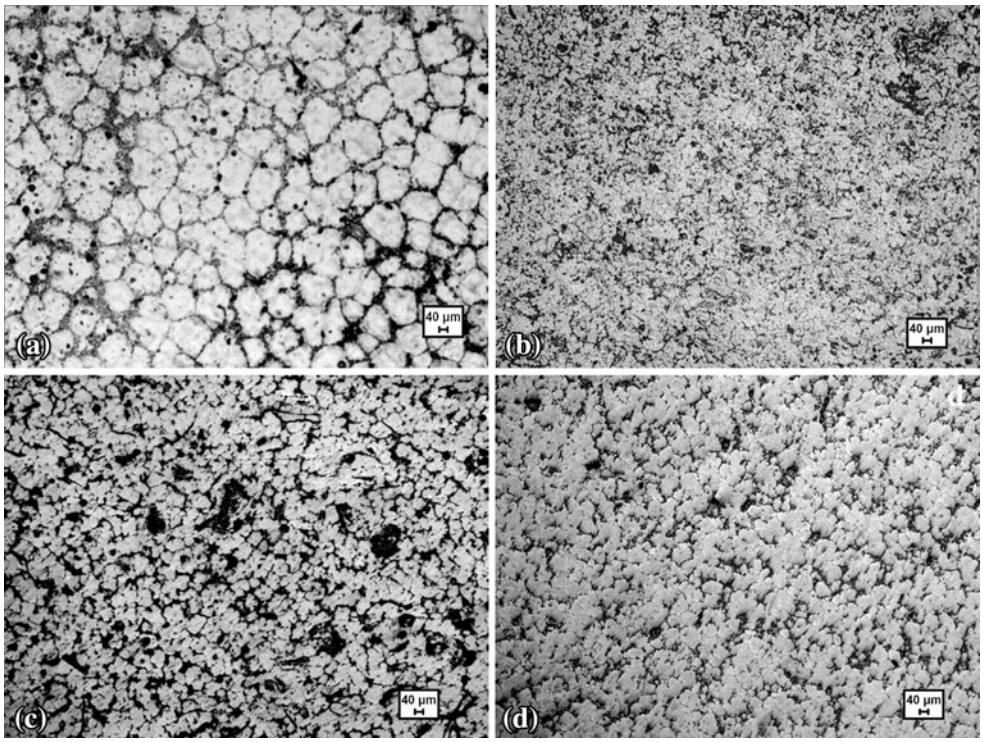

Fig. 2 Optical micrographs of as-cast samples etch with Keller's reagent of (a) 0 (b) 1.5 (c) 3.5, and (d) 6% Mg composite

Mg beyond 1.5%. This is evident from the micrographs in Fig. 2.

At the higher magnification SEM micrograph, the agglomeration of TiB_2 particles at the grain boundary and primary Al_3Sc particles were noticed in all the composites. Few primary particles of 5 μm average size are shown in Fig. 3(a) by arrow of the 3.5 Mg composite. At the center of few grains the primary particles were also noticed. These particles might be the nucleation site for α-Al. TiB_2 particles were observed in varied size range and were distributed in two distinct regions. At the grain boundary co-existence of larger and smaller particles (Fig. 3b) in the form of aggregate is observed. In the present reported composites, particles away from the grain boundary are finer and uniformly distributed as shown in Fig. 3(b) marked C (magnified from the marked region A of Fig. 3a). The agglomeration of TiB_2 particle in varied size is shown in Fig. 3(c) of the magnified region B of Fig. 3(b). A Si particle is also seen in Fig. 3(c) beside the particles aggregate. However, a coarse Al_3(Sc, Zr) particle of different sizes at the grain boundary were only detected in 6 Mg composite shown in Fig. 3(d). SEM/EDX elemental analysis using line scan along AA in Fig. 3(e) shows the composition variation. EDX result shows an increase in Mg at the grain boundary. At the grain boundary edge of the primary particles Mg and Sc contents is significantly higher as compared to the edge toward the grain. A small amount of Zr was detected throughout the particle. From the literature, these particles can be regarded as the combination of Al_3Sc and Al_3(Sc, Zr). However, the precipitates nucleate from the solid solution on aging are extensively studied and reported as Al_3(Sc, Zr) phase in the present studied composition (Ref 17, 20, 22). These precipitates are of $Al_3(Sc_{1-x}, Zr_x)$ type as shown by some investigators.

3.2 Aging Behavior of the As-Cast Composite

3.5 Mg composite sample cast by quenching of investment mold was chosen for the TEM study for detailed analysis as this sample exhibited best combination of properties. Sub-micron size hexagonal particles containing higher Ti and lower Sc shown in Table 2 of the point marked B and distributed uniformly in the matrix are observed as shown in the bright-field TEM image (Fig. 4a). These particles are TiB_2 particles as seen from EDX analysis. Moreover, precipitates of Al_3Sc probably nucleated during solidification marked by arrow in the microstructure in Fig. 4(a). Although as-cast TEM study was not carried out, the shape of the precipitates indicated the precipitation during solidification as evidence from the literature of fine nanosized round Al_3(Sc, Zr) precipitation after aging at 300 °C temperature. EDX analysis of one of the precipitates marked C is shown in Table 2 identified as Sc-rich precipitate. A considerable amount of Ti in this point indicated the TiB_2 adjacent to it. These nanosized TiB_2 particles are being reported possibly for the first time in Al-Sc-Zr alloy. The dark-field image of the Fig. 4(b) is shown in Fig. 4(c) also reveals the presence of nanosized Al_3Sc and Al_3(Sc, Zr) precipitates. Precipitate size is below 12 nm as estimated from the micrograph.

Addition of 1.5% Mg to the composite improved as-cast hardness significantly (Fig. 5a) but with further increase in Mg there is only a small change in the as-cast hardness. The samples were aged isothermally at 300 °C up to 24 h. The change in hardness with time on isothermal aging treatment is shown in Fig. 5(a). The hardness variation of the samples studied at an overaging temperature of 400 °C for the duration of 5 h is shown in Fig. 5(b). The results show that the aging response changes with Mg addition. Mg slows down the aging

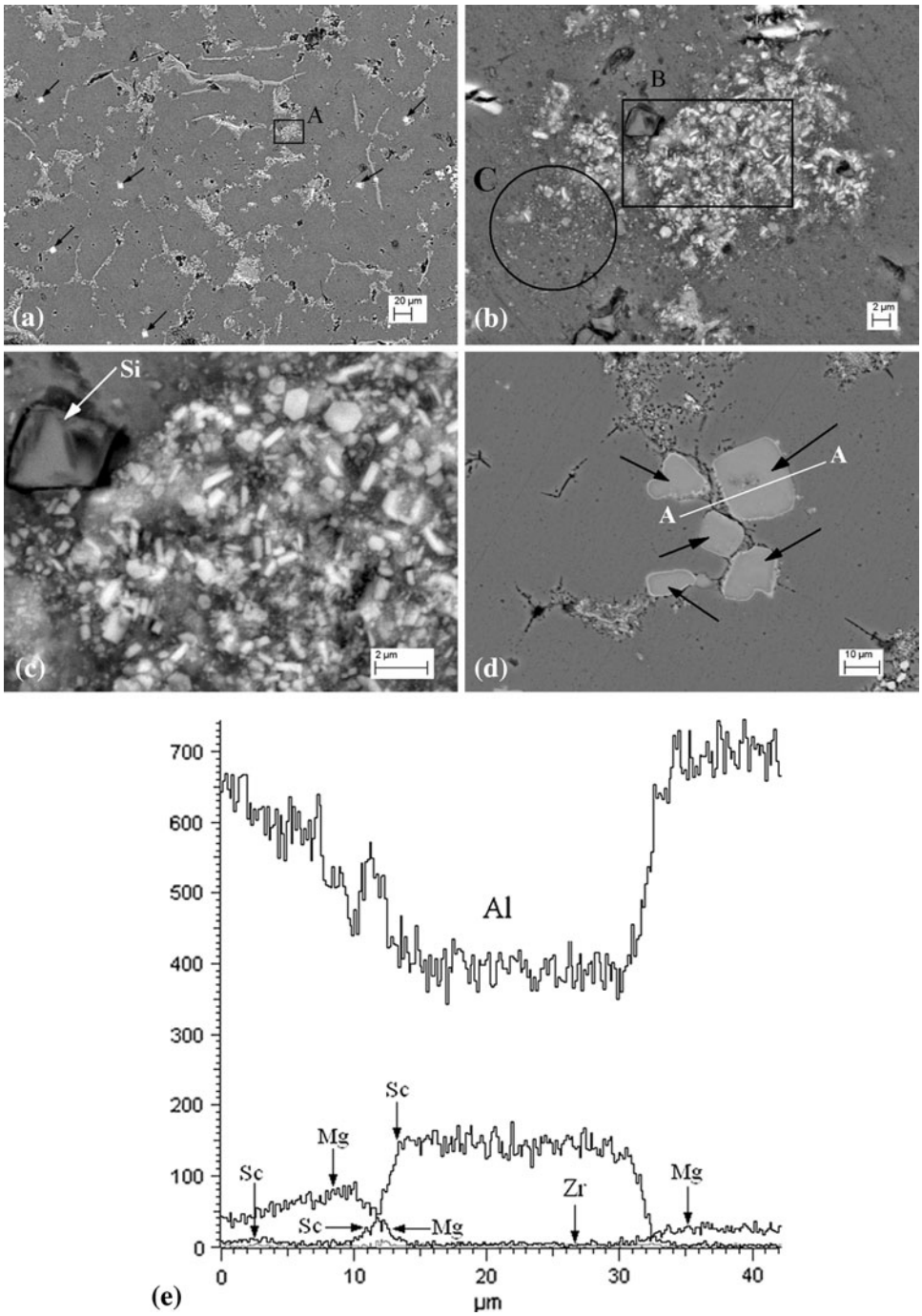

Fig. 3 SEM micrograph of 3.5% Mg as-cast without etch composite samples at (a) low magnification, (b) magnified from the region A of (a), (c) magnified from the region B of (b), (d) 6% Mg composite, and (e) EDAX pattern of the line marked AA on the particles of (d)

Table 2 EDX micro-chemical analysis (in wt.%) of the corresponding point in Fig. 4(a)

Alloy	Mg	Sc	Fe	Si	Ti	Zr	Al
B	0.99 ± 0.03	0.66 ± 0.05	…	…	82.96 ± 1.40	…	15.40 ± 0.53
C	…	5.37 ± 0.08	…	…	64.60 ± 1.33	…	30.03 ± 1.04

response in the beginning. However, the time to reach peak hardness is in between 90 and 150 min at 300 °C and remains unaltered by the change in Mg content. A significant increase in peak hardness was observed at 3.5 Mg content composite (Fig. 5a). All the alloys showed a good response to the aging but the as-cast hardness of magnesium free composite was the lowest of all the composites studied. The phenomenon of overaging is clearly seen at the temperature of 400 °C (Fig. 5b). Figure 5(b) shows that there is a sharp drop of hardness around 100 min and thereafter the hardness value remains practically constant. The retained hardness is higher, higher the magnesium content as shown in Fig. 5(c).

Tensile properties of the composites are shown in Table 3. A substantial increase in strength with relatively low loss in

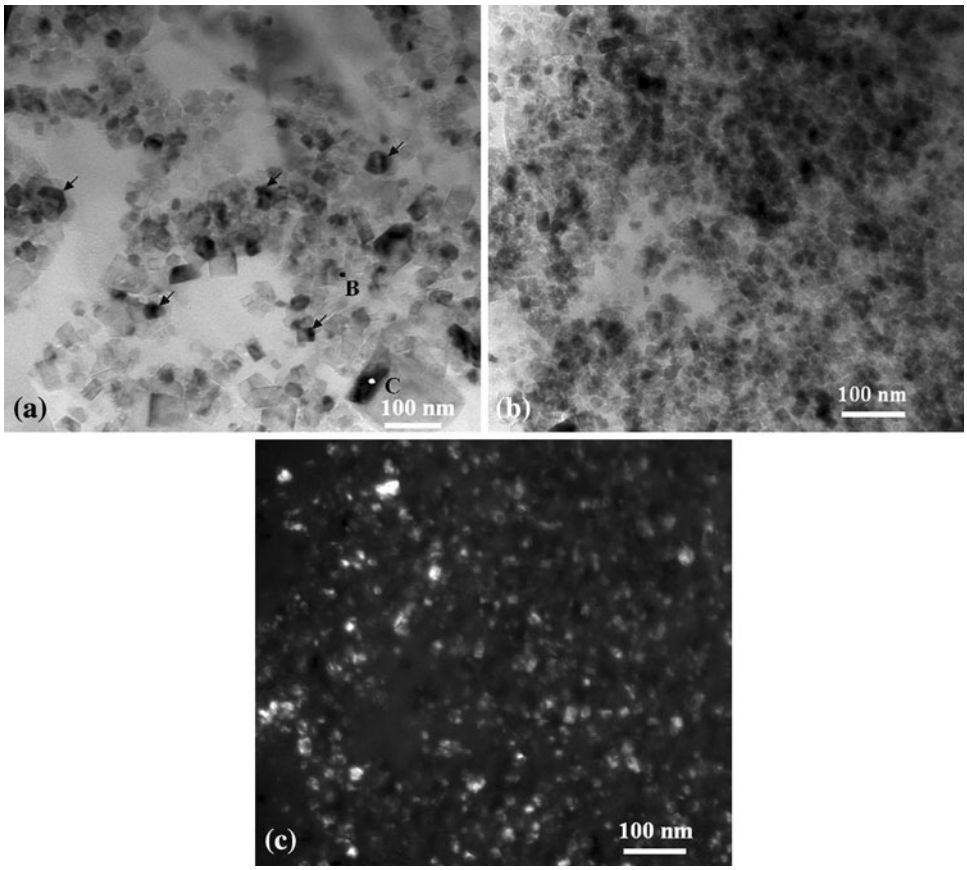

Fig. 4 Bright-field image TEM micrograph of the composite with 3.5% Mg composite showing (a) a cell structure precipitation of TiB_2, (b) the dense and uniform distribution of the TiB_2 particles, and (c) the fine precipitates of Al_3Sc, $Al_3(Sc, Zr)$ in the corresponding dark-field image of (b) aged at 300 °C for 5 h

ductility with addition of 1.5% Mg is noticed in the as-cast material. With further increase of magnesium to 3.5% the strength increased further with loss in ductility. The strength and ductility decreased with increase of magnesium level to 6%. Aging of the samples resulted in a drop in ductility is shown in Table 3. However, the drop in ductility is less pronounced in case of magnesium free composite. For the magnesium-containing composites, the drop in ductility was more pronounced. In the composite with 6% Mg, the improvement of strength is not much and there is a drastic reduction in ductility. Yield strength of all the composite is improved with the addition of Sc.

4. Discussion

The dispersion of the TiB_2 particle is enhanced by the surface tension of the liquid aluminum alloy and the consequent reduction the interfacial energy between particle and matrix. Mg is the preferred addition to aluminum alloys to reduce this interfacial energy between TiB_2 and liquid aluminum. Further, the solute Mg atoms accelerate the nucleation rate of TiB_2 particles during the salt reaction by lowering the interfacial energy and the prevalent low growth rates at lower interfacial energy prevent the clustering of the reinforcing particles (Ref 7). The TiB_2 particles formed promote grain refinement of aluminum alloy. Refinement of grains structure is also observed when Sc is added beyond the eutectic (0.55 wt.% Sc) composition in binary Al-Sc alloys and ternary Al-0.5Sc-0.15Zr alloy (Ref 24). In these alloys the primary $Al_3Sc/Al_3(Sc, Zr)$ precipitation promotes the formation of α-Al nuclei (Ref 25). The presence of TiB_2, Sc, and Zr are the cause of equiaxed grain structure in magnesium free composites studied, as ternary Al-0.3Sc-0.15Zr alloy reveals coarse grain structure (Ref 23). Addition of 1.5% Mg reduced the grain size to much lower levels. However, increase in Mg content further increased the grain size as well as segregation of TiB_2 particles on the grain boundaries. Earlier studies indicate that the maximum Mg that can produce structure free from primary $Al_3Sc/Al_3(Sc, Zr)$ particles is 4.11% (Ref 20) with similar concentration of Sc and Zr as used in this study. A minor joint addition of Sc and Zr reported to refine the grain structure or diminishing dendritic structure in Al-Mg alloy. Singh et al. reported that the grain size remains unchanged up to 4 wt.% Mg. Increase in Mg content to 8 wt.%, primary particles are nucleated and reported to reduce grain size drastically (Ref 20). In this investigation even with Mg-free composite the $Al_3Sc/Al_3(Sc, Zr)$ particles was noticed. The presence of the primary particles indicates that the Sc and Ti have a significant mutual solubility. Reported literature points the simultaneous presence of Sc and Mg in aluminum mutually reduces their solubility during solidification (Ref 22). The drop in the solubility was confirmed by the presence of coarse primary particles in the present investigation of the highest composition of Mg composite. In Fig. 3(d), coarse precipitates of $Al_3Sc/Al_3(Sc, Zr)$ attributed low solubility of Sc

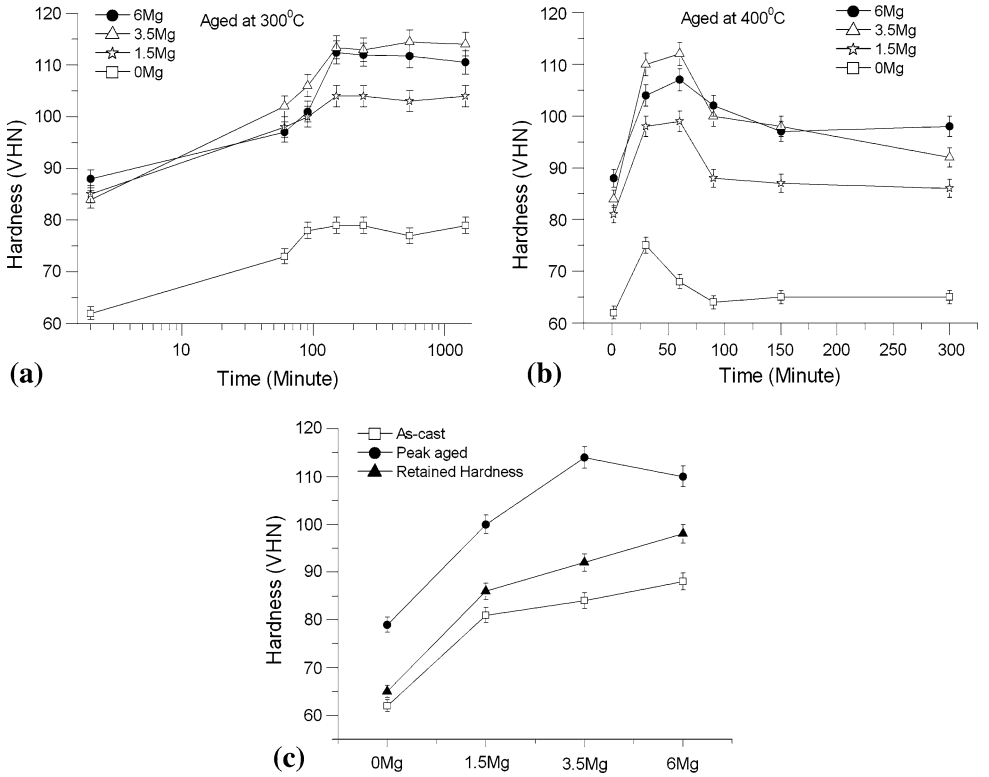

Fig. 5 Hardness variation during isothermal aging at the temperature of (a) 300 °C, (b) 400 °C and the addition of different concentrations of Mg in (c) as cast, peak age, and retained hardness at 400 °C

Table 3 Strength properties of the composites

Casting process	Condition	UTS, MPa	YS, MPa	Hardness, VHN	Elongation, %
0.0 Mg	As cast	138	115	62	14.54
	Peak age	161	143	79	10.14
1.5 Mg	As cast	257	226	81	13.26
	Peak age	284	242	100	07.21
3.5 Mg	As cast	262	245	84	11.41
	Peak age	301	277	114	07.01
6 Mg	As cast	224	157	88	10.70
	Peak age	258	185	110	05.68

in this composition. Coarse primary particles at the grain boundaries 6 Mg composite and fine primary particles in the rest of the present studied composite inside the grain were observed. The fine primary particles are probably responsible for nucleation of the grain. Coarse particles at the grain boundary were pushed into the Sc-rich interdendritic liquid during solidification. Sc-rich melt in the interdendritic space help the growth of the primary particles leading to the coarse particles at the grain boundary.

A significant mutual solubility between Zr, Ti, and Sc reduces the eutectic composition from the binary Al-Al_3Sc (Ref 25). Excess Ti is not expected as it is exhausted by the formation of TiB_2, or aluminide layer on the TiB_2 particles as reported in the literature (Ref 2). X ray diffraction result shows the presence of TiB_2 (Fig. 6) particles. TiB_2 particles were mostly of hexagonal structure as indicated by the XRD peaks and in Fig. 3(c). In the XRD study, Mg_3Al_2 and ZrB_2 phases

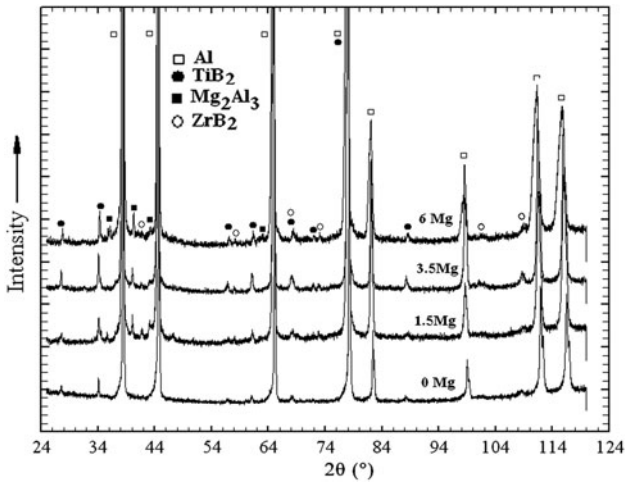

Fig. 6 X-ray diffraction taken from the as-cast samples

were also identified through their weak peaks as shown in Fig. 6. It is reported that Zr is a strong boride former and promotes the formation of (Ti, Zr)B_2 (Ref 13) by replacing Ti in Al_3Ti layer on the boride particle (Ref 15). An appreciable substitution of Ti by Sc in the Al_3(Sc, Ti) phase might take place giving rise to an increase in the number of nucleation sites for TiB_2 leading to the production of nanosized precipitates as is evident from the TEM study (Fig. 4a). Mg and Zr as solute atoms in aluminum reduce the average size of the TiB_2 particles (Ref 13) thus producing larger number of these particles.

Similarly, presence of Sc and Zr reduces the size of these reinforcement particles further. The mechanism of formation of such nanosized TiB_2 in this complex alloy composition needs a detailed investigation.

As-cast hardness result of the entire composite showed a significant improvement except the absence of Mg. In addition to that, solid solution hardening effect on increasing in Mg has been observed. The reduction in hardness in the 6 Mg content composite could be the precipitation of Mg_5Al_8 type phase, which is known to soften Al-Mg alloy and the increase in grain size. Result of the peak hardness indicated that minimum amount of Mg is required for combine effect of solid solution of Mg and fine nanosized $Al_3(Sc, Zr)$ or Al_3Sc precipitates. At the temperature of 400 °C hardness reduction up to 1.5 h was not observed. Rapid loss in the hardness value indicated beyond 1.5 h. At high temperature, more Mg is in solid solution might increase in the hardness at the beginning and loss in the hardness at longer time period was probably the annihilation of the dislocations as the coarsening of the nanosized precipitates at 5 h was not detected in the TEM study.

Addition of Mg promotes the formation of TiB_2 and reduces the size of the particles in these composites. Dispersion of the particles uniformly in presence of Mg improves the strength properties without loss of ductility. Increase in strength with increase in Mg could be explained as the solid solution affect as the ductility of the material reduced. A minor amount of Mg resulted in dispersion of particles uniformly. For obtaining the optimum mechanical properties, the combined effect of solid solution strengthens with the addition of Mg; age hardening with Sc and Zr and TiB_2 particles needs to be examined. Experimental investigation of the present report showed that the Mg content should be less than 6 and more or equivalent to 3.5 wt.% of Mg with Al0.3Sc0.15Zr alloy. Consistent tensile properties of the each tested sample is attributed to the formation of nanosized TiB_2 and $Al_3Sc/Al_3(Sc, Zr)$ in these composite material.

5. Conclusion

1. Grain size of the TiB_2 reinforced Al-Sc-Zr composite mainly due to the combine effect of TiB_2 particles and a minor addition of Sc and Zr. A minor addition of Mg reduces grain size drastically. Further increase in Mg content, the grain size increases by increasing Sc precipitation during solidification and push the TiB_2 and coarse $Al_3Sc/Al_3(Sc, Zr)$ particles to the grain boundary.
2. The aging response is unchanged with the variation in Mg at the lower level of Mg addition, at the beginning poor response in aging of the composition of 6% Mg. Time to reach peak age hardness is also unaffected. Thus, Mg addition does not alter the precipitation process during aging of the composites. The 6% Mg containing composite soften by the precipitation of Mg_5Al_8 type phase couple with the reduction of mutual solubility of Mg and Sc reduces the aging response at the beginning and peak age condition.
3. A minor addition of Mg, distribution of particles is more or less uniform and cluster of particles with increase in Mg content. The strength of the material initially increases with the increase in Mg and decrease substantially at 6% Mg. The optimum strength lies in between 3.5 and 6.5% Mg as 3.5% Mg-containing composite is having better ductility and strength. In the presence of the nanosized $Al_3Sc/Al_3(Sc, Zr)$ and TiB_2, strength and ductility of the composites is increased.

References

1. M.D. Salvador, V. Amigó, N. Martinez, and C. Ferrer, Development of Al–Si–Mg Alloys Reinforced with Diboride Particles, *J. Mater. Process. Technol.*, 2003, **143–144**, p 598–604
2. A. Mandal, B.S. Murty, and M. Chakraborty, Sliding Wear Behaviour of T6 Treated A356–TiB_2 In-Situ Composites, *Wear*, 2008, **265**, p 1606–1618
3. Y. Zhang, N. Ma, H. Wang, Y. Le, and X. Li, Damping Capacity of Insitu TiB_2 Particulates Reinforced Aluminium Composites With Ti Addition, *Mater. Des.*, 2007, **28**, p 628–632
4. J. Fjellstedt and A.E.W. Jarfors, On the Precipitation of TiB_2 in Aluminium Melts from the Reaction with KBF_4 and K_2TiF_6, *Mater. Sci. Eng. A*, 2005, **413–414**, p 527–532
5. K.V.S. Prasad, B.S. Murty, P. Pramanik, P.G. Mukunda, and M. Chakraborty, Reaction of Fluoride Salts With Aluminium, *Mater. Sci. Technol.*, 1996, **12**, p 766–770
6. B.S. Murty, S.A. Kori, K. Venkateswarlu, R.R. Bhat, and M. Chakraborty, Manufacture of Al-Ti-B Master Alloys by the Reaction of Complex Salts With Molten Aluminium, *J. Mater. Process. Technol.*, 1999, **89–90**, p 152–158
7. A. Jha and C. Dometakis, The Dispersion Mechanism of TiB_2 Ceramic Phase in Molten Aluminium and Its Alloys, *Mater. Des.*, 1997, **18**, p 297–301
8. T. Fan, G. Yang, and D. Zhang, Thermodynamic Effect of Alloying Addition on In-Situ reinforced TiB_2/Al Composites, *Metall. Mater. Trans.*, 2005, **36A**, p 225–233
9. S. Lakshmi, L. Lu, and M. Gupta, In Situ Preparation of TiB_2 Reinforced Al Based Composites, *J. Mater. Process. Technol.*, 1998, **73**, p 160–166
10. P.S. Mohanty and J.E. Gruzleski, Mechanism of Grain Refinement in Aluminium, *Acta Met. Mater.*, 2005, **43**, p 2001–2012
11. Y.M. Youssef, R.J. Dashwood, and P.D. Lee, Effect of Clustering on Particle Pushing and Solidification Behaviour in TiB_2 Reinforced Aluminium PMMCs, *Composites A*, 2005, **36**, p 747–7632
12. T. Srithanan and H. Li, Optimizing the Composition of Master Alloys for Grain Refining Aluminium, *Scripta Mater.*, 1996, **35**, p 1053–1056
13. H. Li, T. Sritharam, Y.M. Lam, and N.Y. Leng, Effects of Processing Parameters on the Performance of Al Grain Refinement Master Alloys Al-Ti and Al-B in Small Ingots, *J. Mater. Process. Technol.*, 1997, **66**, p 253–257
14. P.L. Schaffer and A.K. Dahle, Settling Behaviour of Different Grain Refiners in Aluminium, *Mater. Sci. Eng. A*, 2005, **413–414**, p 373–378
15. A.M. Bunn, P. Schumacher, M.A. Kearns, C.B. Boothroyd, and A.L. Greer, Grain Refinement in Aluminium Melts: A Study of the Mechanisms of Poisoning by Zirconium, *Mater. Sci. Technol.*, 1999, **15**, p 1115–1123
16. A.F. Norman, P.B. Prangnell, and R.S. Mcewen, The Solidification Behaviour of Dilute Aluminium-Scandium Alloys, *Acta Mater.*, 1998, **46**, p 5715–5732
17. N.A. Belov, A.N. Alabin, D.G. Eskin, and V.V. Istomin-Kastrovskii, Optimization of Hardening of Al-Zr-Sc Cast Alloys, *J. Mater. Sci.*, 2006, **41**, p 5890–5899
18. N. Blake and M.A. Hopkins, Constitution and Age Hardening of Al-Sc Alloys, *J. Mater. Sci*, 1985, **20**, p 2861–2867
19. Z. Yin, Q. Pan, Y. Zhang, and F. Jiang, Effect of Minor Sc and Zr on the Microstructure and Mechanical Properties of Al-Mg Based Alloys, *Mater. Sci. Eng.*, 2000, **A280**, p 151–155
20. V. Singh, K.S. Prasad, and A.A. Gokhale, Microstructure and Age Hardening Response of Cast Al-Mg-Sc-Zr Alloys, *J. Mater. Sci.*, 2004, **39**, p 2861–2864
21. K. Venkateswarlu, L.C. Pathak, A.K. Roy, G. Das, P.K. Verma, M. Kumar, and R.N. Ghosh, Microstructure, Tensile Strength and Wear Behaviour of Al-Sc Alloy, *Mater. Sci. Eng. A*, 2004, **383**, p 374–380

22. J. Røyset and N. Ryum, Scandium in Aluminium Alloys, *Int. Mater. Rev.*, 2005, **50**, p 19–44
23. A.K. Lohar, B.N. Mondal, and S.C. Panigrahi, Influence of Cooling Rate on the Microstructure and Ageing Behaviour of As-Cast Al-Sc-Zr Alloy, *J. Mater. Process. Technol.*, 2010, **210**, p 2135–2141
24. A.K. Lohar, B. Mondal, D. Rafaja, V. Klemm, and S.C. Panigrahi, Microstructure Investigation of As-Cast and Annealed Al-Sc and Al-Sc-Zr Alloys, *Mater. Charact.*, 2009, **60**, p 1387–1394
25. Z. Liu, Z. Li, M. Wang, and Y. Weng, Effect of Complex Alloying of Sc, Zr and Ti on the Microstructure and Mechanical Properties of Al–5 Mg Alloys, *Mater. Sci. Eng. A*, 2008, **483–484**, p 120–122